A Global View of Non-Gaussian SST Variability

Philip Sura and Prashant D. Sardeshmukh

CIRES Climate Diagnostics Center, University of Colorado
and
NOAA Earth System Research Laboratory
Boulder, Colorado

July 24, 2007

Journal of Physical Oceanography
(in press)

Corresponding author address:
Philip Sura
NOAA-ESRL and CIRES Climate Diagnostics Center, R/PSD1
325 Broadway, Boulder, CO 80305-3328
Phone: (303) 497-4426, Fax: (303) 497-6449
E-mail: Philip.Sura@noaa.gov

Abstract

The skewness and kurtosis of daily sea surface temperature (SST) variations are found to be strongly linked at most locations around the globe in a new high-resolution observational dataset, and are analyzed in terms of a simple stochastically forced mixed-layer ocean model. The predictions of the analytic theory are in remarkably good agreement with observations, strongly suggesting that a univariate linear model of daily SST variations with a mixture of SST-independent (additive) and SST-dependent (multiplicative) noise forcing is sufficient to account for the skewness-kurtosis link. Such a model of non-Gaussian SST dynamics should be useful in predicting the likelihood of extreme events in climate, as many important weather and climate phenomena, such as hurricanes, ENSO, and the NAO depend on a detailed knowledge of the underlying local SSTs.

1. Introduction

The atmosphere-ocean system exhibits natural variability on time scales ranging from minutes to millennia. Given the larger density and heat capacity of the ocean, the system can be thought of as a slowly varying system, the ocean, coupled to a rapidly varying system, the atmosphere. This time scale separation has been extensively used to study atmosphere-ocean interactions. The most general formulation of this idea, *stochastic climate models*, was introduced by Hasselmann (1976) and is based on a Brownian motion analog: the observed red spectrum of oceanic fluctuations is a consequence of the amplification of the low-frequency part of rapidly decorrelating stochastic weather fluctuations. The formal derivation of this fast-slow time scale interaction is straightforward. For example, the heat budget equation for sea surface temperature T_o, defined as an average over the mixed-layer depth *h* (see, e.g., Frankignoul 1985) is:

$$\frac{\partial T_o}{\partial t} = \underbrace{-\ \mathbf{v}_o \bullet \nabla T_o}_{A} \ + \underbrace{\frac{Q}{\rho C h}}_{B} \ - \underbrace{\frac{w_e}{h}(T_o - T_o^b)}_{C} \ + \underbrace{\kappa \nabla^2 T_o}_{D} \ \equiv \ F \ , \tag{1}$$

where the rate of change of T_o is governed by advection through ocean currents (A), surface heat fluxes (B), vertical entrainment (C), and horizontal mixing (D). Here $\mathbf{v}_o$ is the horizontal velocity in the mixed-layer, Q is the heat flux through the sea surface, ρ and C are the density and heat capacity of sea water, w_e and T_o^b are the vertical velocity and temperature just below the mixed-layer, and κ is the horizontal mixing coefficient. F denotes the sum of all terms. Note that all of these terms are directly or indirectly affected by atmospheric quantities like winds and temperatures. For small temperature anomalies T_o' a Taylor expansion of the heat flux F with respect to $T_o = \overline{T_o} + T_o'$ yields

$$\frac{\partial T_o'}{\partial t} = \frac{\partial F}{\partial T_o} T_o' + F' \quad , \tag{2}$$

where it is assumed that the evolution of the mean SST $\overline{T_o}$ is balanced by the mean heat flux $\overline{F}$. Because the heat flux anomaly F' is to a large degree due to rapid atmospheric fluctuations, it may be represented as noise η. The derivative $\partial F / \partial T_o$, on the other hand, is usually represented by a constant parameter –λ. That is, the effect of atmospheric forcing on sea surface temperature (SST) anomalies T_o' is often represented by a simple stochastic driving of the oceanic mixed-layer,

$$\frac{\partial T_o'}{\partial t} = -\lambda T_o' + \eta \tag{3}$$

(Hasselmann 1976; Frankignoul and Hasselmann 1977, hereafter FH77), where λ is a rate coefficient representing the transfer of heat from the slowly evolving mixed-layer heat anomaly, and η is Gaussian white-noise representing the heat fluxes due to rapidly varying weather fluctuations. The *e*-folding time scale of SST variability is thus τ = 1/λ. Such a simple univariate linear system has been surprisingly successful in explaining many features of midlatitude SST variability (e.g., Frankignoul and Hasselmann 1977; Reynolds 1978; Hall and Manabe 1997, and many others).

The classical stochastic view in (3) implies that T_o' has a Gaussian probability density function (PDF). Indeed, temporally (e.g., monthly, seasonally, or even yearly) or spatially (e.g., several degrees) averaged SST anomalies are nearly Gaussian. We expect this partly from the Central Limit Theorem (e.g., Gardiner 2004; Paul and Baschnagel 1999) to the extent that it is applicable to time-averaged quantities. On daily scales, however, observations from Ocean Weather Stations (OWS) show that the PDFs of SST are significantly non-Gaussian (Sura et al. 2006). So far (to our knowledge), no systematic attempt has been made to globally map and discuss the non-Gaussian features of daily SST anomalies.

One reason for interest in the non-Gaussianity of rapidly sampled SST anomalies is that the analysis of deviations from Gaussianity, or anomalous statistics, can shed light on the basic mechanisms of SST variability [and of other physical processes; see, e.g., Peinke et al. (2004) or Sura et al. (2005) for a more general discussion]. Sura et al. (2006) analyzed the non-Gaussianity at several OWS and found it to be consistent with a univariate multiplicative noise model that also considers stochastic fluctuations in the relaxation coefficient λ in (3). The classical FH77 hypothesis assumes that λ is a constant. It has been shown (Sura et al. 2006; Blaauboer et al. 1982; Müller 1987), however, that rapid fluctuations in λ, as expected from the gustiness of sea surface winds, cannot be ignored. If we replace λ in (3) with $\lambda = \overline{\lambda} + \lambda'$, where $\overline{\lambda}$ is constant and λ' is white-noise, then $\lambda' T_0'$ is a noise term whose amplitude depends linearly on the amplitude of the SST anomaly T_0', and is thus a linear "multiplicative" noise term.

In this paper we use a multiplicative noise model, derived directly from the basic mixed-layer Eq. (1), to explain a remarkable global property of non-Gaussian SST variability found in a daily sampled SST dataset, namely that the skewness and kurtosis of the daily SST variations are closely linked at most locations around the globe. Our principal interest here is in a global characterization of non-Gaussian SST variability, and not in the detailed SST anomaly budget at specific locations [as has been done in many papers, including Sura et al. (2006)]. We are approaching the problem of SST variability more in the light of statistical mechanics. In other words, we want to understand an observed global constraint on non-Gaussian SST variability by looking at a large ensemble of related local quantities.

The results from the SST dataset are presented in section 2. In section 3 we present a simple theory of the mixed-layer dynamics (1) that links the skewness and kurtosis of the SST variations. Its relevance to observations is discussed in section 4. Finally, section 5 provides a summary and discussion.

2. Observations

As already mentioned in the introduction, PDFs are useful diagnostic measures of the dynamics of stochastic systems. In particular, deviations from Gaussianity can shed light on the underlying dynamics (e.g., Peinke et al. 2004; Sura et al. 2005; Sura et al. 2006; Sura and Newman 2007). Here, we analyze the higher moments (skewness and kurtosis) of daily SST anomalies. We first present global maps of skewness and kurtosis, and then investigate the remarkable link between these higher moments as revealed on a scatter plot.

a. Data

Recently, NOAA produced a blended analysis of daily SST fields based on infrared satellite data from the Advanced Very High Resolution Radiometer (AVHRR) and in situ data from ships and buoys (Reynolds et al. 2007). The analysis was performed using optimum interpolation with a separate step to correct satellite biases relative to the in situ data. The in situ data were obtained from the International Comprehensive Ocean-Atmosphere Data Set (ICOADS; http://icoads.noaa.gov/). This NOAA daily SST analysis is available on a 0.25-degree latitude/longitude grid from January 1985 to the present. A more detailed description of the dataset and analysis procedure can be found in Reynolds et al. (2007). SST anomalies were calculated by subtracting the daily climatology and linear trend from the full daily values. We then analyzed the extended summer (May-October) and extended winter (November-April) seasons.

b. Higher moments: skewness and kurtosis

As we cannot accurately estimate the full PDF at every grid-point, we use skewness (third moment) and kurtosis (fourth moment) to characterize the overall shape of the PDF. If the standard deviation of SST anomalies T_o' is denoted by σ, the skewness (*skew*) and kurtosis (*kurt*) become

$$skew \equiv \frac{\langle T_o'^3 \rangle}{\sigma^3}, \quad kurt \equiv \frac{\langle T_o'^4 \rangle}{\sigma^4} - 3. \tag{4}$$

Skewness is a measure of asymmetry of a PDF. If the left tail is heavier (more pronounced) than the right tail, the PDF has negative skewness. If the reverse is true, it has positive skewness. If the PDF is symmetric, it has zero skewness. Kurtosis (or more accurately, "excess kurtosis", since we subtract the kurtosis of 3 for a Gaussian distribution) measures the excess probability (fatness) in the tails, where excess is defined in relation to a Gaussian distribution. The standard errors $\sigma_{\mathrm{skew/kurt}}$ of skewness and kurtosis are approximately $\sigma_{skew} = \sqrt{6 / N_{in}}$ and $\sigma_{kurt} = \sqrt{24 / N_{in}}$ respectively, where N_{in}

is the effective number of independent observations. We remember that ± *one* standard error corresponds to approximately the 68% confidence interval, and ± *two* standard errors to the 95% confidence interval. To obtain a globally typical estimate of N_{in} , we note that since we use 21 years of data, the total number of observations N at each grid point in each extended season is about 3800. If we now make the reasonable assumption that SST anomalies have a decorrelation time scale of about a month, we get $\sigma_{skew} \approx 0.2$ and $\sigma_{kurt} \approx 0.4$. This is a conservative estimate, because it ignores the spatial coherence of the moments. That is, if we see large coherent regions in the geographical maps of the moments, we may "trust" them even if they do not satisfy local significance criteria. Therefore, we will in the following show the full global maps of SST anomaly moments (skewness and kurtosis) equatorward of 65° North and South (to avoid regions with sea ice) before turning our attention to the standard errors again in a scatter plot of skewness versus kurtosis.

The skewness of SST anomalies in the extended summer (upper panel) and winter (lower panel) seasons is shown in Fig. 1. It shows a rich structure in both seasons, whose detailed investigation is beyond the scope of this paper. It is, nonetheless, worth mentioning that the skewness (in both seasons) in this gridded dataset matches that of independent SST observations at colocated Ocean Weather Stations (Sura et al. 2006). By independent we mean that in situ Ocean Weather Station (OWS) data are not blended into this gridded dataset (starting 1985), because almost all OWS were unfortunately abandoned by 1982 [see Dinsmore (1996) for a brief history of Ocean Weather Stations].

In particular the positive in situ skewness at OWS[1] P, N, K, and the negative one at OWS[1] V match the skewness at nearby gridpoints in this dataset [see Sura et al. (2006) for a detailed discussion of the PDFs at several OWS]. Therefore, we are confident that the moments in this SST dataset are reliable and not an artifact of the satellite retrieval or optimal interpolation procedures.

The kurtosis of SST anomalies in the extended northern summer (upper panel) and winter (lower panel) seasons is shown in Fig. 2. Again, without discussing the maps in detail, we observe a rich structure in both seasons.

Now the reader may ask, rightfully, what the value of Figs. 1 and 2 actually is, if we do not discuss the structures in detail (at least not in this paper). The global value becomes obvious as soon as we plot the kurtosis as function of skewness, as done in Fig. 3. As already mentioned, we are interested in a global view of non-Gaussian SST variability. That is, we are not interested here in the detailed dynamics at a given point, but in global constraints induced by local dynamics. In a way we are applying the ideas of statistical mechanics to SST variability: We are looking to relate the local ("microscopic") properties of SST variability to global ("macroscopic") properties of the upper ocean temperature. In the context of non-Gaussian SST variability, what kind of property may be useful to link local dynamics to a global constraint? As we will see and discuss in the remainder of this paper, the functional relationship between skewness and kurtosis gives us an excellent tool to explore a link between local and global dynamics.

Fig. 3 shows a scatter plot of kurtosis as a function of skewness for all data points equatorward of 65° North and South. Here we have not made any distinction between

---

[1] OWS P: 50°N, 145°W; OWS N: 30°N, 140°W; OWS K: 45°N, 16°W; OWS V: 34°N, 164°W.

extended summer and winter, but plotted all available points; there are about 1.1 million data points in the scatter plot. The estimated local 95% confidence intervals on the values are indicated in the upper right corner of the figure.

The solid line in Fig. 3 shows a lower parabolic bound on kurtosis in our dataset: $kurt \geq \frac{3}{2}\, skew^2$. Remarkably, almost without exception, all of the data points lie above this parabola. This is evidently a very strong constraint on the non-Gaussian character of the SST variability. Note that this is a stronger lower bound than the more general statistical bound valid in any system: $kurt \geq skew^2 - 2$ (e.g.,Wilkins 1944). At this point, to our knowledge, there is no obvious dynamical reason why SST variability should behave this way. Therefore, we ask the obvious question. Can we explain the observed global ("macroscopic") constraint on the non-Gaussianity of SST variability by local ("microscopic") dynamics? Posed differently, can we learn something fundamental about local SST variability by examining and explaining the observed global constraint? As it turns out in the remaining sections, we definitely can.

3. Theory

In the previous section we showed that daily SST anomalies obey a non-Gaussian distribution. In particular, we showed that there is a striking parabolic functional relationship between skewness and kurtosis. We next present a theory that explains this remarkable feature of observed SST anomalies.

a. Basic equations

The starting point for our theory is the mixed-layer equation (1). We already noticed [Eq. (2)] that for small temperature anomalies T_o' a Taylor expansion of the heat flux with respect to $T_o = \overline{T_o} + T_o'$ yields

$$\frac{\partial T_o'}{\partial t} = \frac{\partial \bar{F}}{\partial T_o} T_o' + \frac{\partial F'}{\partial T_o} T_o' + F' + R' . \tag{5}$$

Here, in contrast to Eq. (2), we just replaced the full heat flux F with its constituents $\bar{F} + F'$ and added a residual term R' to represent all the processes not included in our mixed-layer equation (1). This, at first glance, trivial replacement is done to highlight the fact that the derivative $\partial F / \partial T_o$ actually consists of two terms: the constant term $\partial \bar{F} / \partial T_o$ and the rapidly varying term $\partial F' / \partial T_o$. The constant term justifies the introduction of the constant feedback parameter –λ (as in FH77). However, as described in Sura et al. (2006), the rapidly varying term cannot be neglected as done in many studies (e.g., in FH77). If we now implement the same approximations made to replace $\partial \bar{F} / \partial T_o$ with –λ, namely that $F = \bar{F} + F'$ is a linear function of T_o (see, e.g., FH77 and Sura et al. 2006), in both the constant and the rapidly varying derivative we get the following equation for SST anomalies:

$$\frac{\partial T_o'}{\partial t} = -\lambda T_o' - \phi F' T_o' + F' + R' + \phi \overline{F'T'} , \tag{6}$$

with the locally constant parameters –λ and –ϕ, and the rapidly varying forcing terms F' and R'. If we now assume that the rapidly varying terms F' and R' can be approximated as independent, zero mean Gaussian white-noise processes with amplitudes $\sigma_{F'}$ and $\sigma_{R'}$, $\overline{F'(t)F'(t')} = (\sigma_{F'})^2 \delta(t-t')$, $\overline{R'(t)R'(t')} = (\sigma_{R'})^2 \delta(t-t')$, (6) becomes a stochastic differential equation (SDE) for SST anomalies T_o'. Note that (6) is an SDE with state-dependent (multiplicative) noise because the noise F' is multiplied by the SST anomaly T_o' and, therefore, depends on the state of the system T_o' [for a detailed discussion of SDEs see for example Gardiner (2004), Horsthemke and Léfèver (1984), Kloeden and Platen (1992), or any other textbook on SDEs]. For our purpose, the only important detail to recognize is that the SDE (6) has to be interpreted in the Stratonovich sense. In the Stratonovich calculus the deterministic drift term $-\lambda$ has to be replaced by the effective drift $-\lambda_{eff} \equiv -\lambda + \frac{1}{2}\left(\phi\sigma_{F'}\right)^2$, which is the sum of the deterministic drift and the noise-induced drift. The noise-induced drift appears in Stratonovich systems because then the time mean of the multiplicative noise term, here $-\phi\overline{F'T_o'}$, is not zero. This is also why one needs to introduce an additional mean forcing $\phi\overline{F'T_o'}$ in (6) to ensure that the time mean of T_0' is zero. This is a simple stochastic renormalization procedure, which does not impact the dynamics of SST variability. Without going into details, we note that Stratonnovich calculus is applicable in continuous physical systems such as the ocean and atmosphere in which rapidly fluctuating quantities with small but finite correlation times are approximated as white-noise. Readers interested in more details should consult one of the available textbooks (see above). The remainder of this paper is generally understandable without a detailed knowledge of SDEs.

The multiplicative noise system (6) has one important property of interest here. In general, the SDE (6) will produce non-Gaussian statistics. Indeed, a version of Eq. (6) has been already used in Sura et al. (2006) to model observed non-Gaussian SST anomalies at several OWS locations. That was, however, a local endeavor focusing on detailed local dynamics. The goal of this paper is to explore if (6) is globally relevant, neglecting detailed local conditions as much as possible. Because we looked at the functional form of kurtosis versus skewness in Fig. 3, the next step is to calculate skewness and kurtosis from the SDE (6).

b. Equation for the moments: skewness and kurtosis

The Fokker-Planck equation (e.g., Gardiner 2004; Horsthemke and Léfèver 1984) for the stationary PDF p of SST anomalies $T_0' \equiv x$ governed by (6) may be written

$$0 = \frac{d}{dx}\left[\lambda_{eff} x p\right] + \frac{1}{2}\frac{d^2}{dx^2}\left[\left(\sigma_{F'}{}^2 + \sigma_{R'}{}^2 + \phi^2 \sigma_{F'}{}^2 x^2 - 2\phi\sigma_{F'}{}^2 x\right) p\right]. \tag{7}$$

Expressions for the moments $< x^n >$ of may be obtained from (7) by multiplying by powers of x and integrating by parts. This yields $< x > \ = \ 0$ for the first moment (n = 1), and the following expression for the higher moments ($n \geq 2$):

$$\left[\lambda_{eff} - \frac{n-1}{2}(\phi\sigma_{F'})^2\right] < x^n > = -(n-1)\ \phi\ \sigma_{F'}{}^2 < x^{n-1} > \ + \ \frac{n-1}{2}\ \left(\sigma_{F'}{}^2 + \sigma_{R'}{}^2\right) < x^{n-2} > \ . \tag{8}$$

In particular, the second, third and fourth moments are

$$\begin{aligned} < x^2 > \ &= \ \left(\sigma_{F'}{}^2 + \sigma_{R'}{}^2\right) / \left[2\lambda_{eff} - (\phi\sigma_{F'})^2\right], \\ < x^3 > \ &= \ -2\phi\sigma_{F'}{}^2 < x^2 > / \left[\lambda_{eff} - (\phi\sigma_{F'})^2\right], \\ < x^4 > \ &= \ \left[-3\phi\sigma_{F'}{}^2 < x^3 > + (3/2)\left(\sigma_{F'}{}^2 + \sigma_{R'}{}^2\right) < x^2 >\right] / \left[\lambda_{eff} - (3/2)(\phi\sigma_{F'})^2\right]. \end{aligned} \tag{9}$$

Now we divide the equation for $< x^4 >$ by $< x^2 >^2 \equiv \sigma^4$ and use the definitions of skewness and kurtosis in (4) to obtain

$$kurt + 3 = \frac{1}{\left(\lambda_{eff} - \frac{3}{2}(\phi\sigma_{F'})^2\right)}\left[\frac{-3\phi\sigma_{F'}{}^2 skew}{< x^2 >^{1/2}} + \frac{3}{2}\frac{\left(\sigma_{F'}{}^2 + \sigma_{R'}{}^2\right)}{< x^2 >}\right] \ . \tag{10}$$

If we now replace $-3\phi\sigma_{F'}{}^2 skew/<x^2>^{1/2}$ with ${}^3\!/_2\left(\lambda_{eff}-(\phi\sigma_{F'})^2\right)skew^2$ (using the expression for $<x^3>$) and $\left(\sigma_{F'}{}^2+\sigma_{R'}{}^2\right)/<x^2>$ with $\left(2\lambda_{eff}-(\phi\sigma_{F'})^2\right)$ (using the expression for $<x^2>$) we obtain our final equation

$$kurt+3=\frac{{}^3\!/_2}{\left(-\lambda_{eff}+{}^3\!/_2(\phi\sigma_{F'})^2\right)}\left[\left(-\lambda_{eff}+(\phi\sigma_{F'})^2\right)skew^2-\left(2\lambda_{eff}-(\phi\sigma_{F'})^2\right)\right]. \qquad (11)$$

We already see, without discussing (11) in detail (that is done in the next section), that the kurtosis is a function of the skewness squared. Thus, just at first glance, we notice a structure that might explain the parabolic constraint in Fig. 3.

4. Theory versus observations

Having derived Eq. (11) for the kurtosis as a function of the skewness we now move on to explore in detail if (11) is able to explain the structure shown in Fig. 3. To ease the following discussion, we use the following nomenclature for (11): $kurt = A\ skew^2 + B$, with the factor *A,*

$$A=\frac{{}^3\!/_2\left(-\lambda_{eff}+(\phi\sigma_{F'})^2\right)}{\left(-\lambda_{eff}+{}^3\!/_2(\phi\sigma_{F'})^2\right)}\ , \qquad (12)$$

and the vertical offset *B,*

$$B=\frac{3\left(-\lambda_{eff}+{}^1\!/_2(\phi\sigma_{F'})^2\right)}{\left(-\lambda_{eff}+{}^3\!/_2(\phi\sigma_{F'})^2\right)}-3\ . \qquad (13)$$

Let us first discuss the factor *A*. The first observational fact to notice is that the strength of the multiplicative noise $(\phi\sigma_{F'})^2$ is usually relatively weak compared to λ_{eff} (Sura et al. 2006), so that the multiplicative noise contribution to the drift can be neglected in a first-order approximation: $-\lambda_{eff} + (\phi\sigma_{F'})^2 \approx -\lambda_{eff} + \frac{3}{2}(\phi\sigma_{F'})^2 \approx -\lambda$. Therefore, $A \approx \frac{3}{2}$ for weak multiplicative noise. At this point it is important to recognize that this *weak-multiplicative-noise* approximation is not equivalent to having *no multiplicative noise* at all. For no multiplicative noise *skew* = 0, and $kurt = A\ skew^2 + B$ collapses to $kurt = 0$. We also notice that this weak-multiplicative-noise approximation provides us with a lower-limit of *A*, because $\left(-\lambda_{eff} + (\phi\sigma_{F'})^2\right) / \left(-\lambda_{eff} + \frac{3}{2}(\phi\sigma_{F'})^2\right) \geq 1$. Note that, for the fourth moment to exist [see (9)], there is an upper limit for he strength of the multiplicative noise: $(\phi\sigma_{F'})^2 < \left(\frac{2}{3}\right)\lambda_{eff}$. Thus, in general $A \geq \frac{3}{2}$. This gives us exactly the shape of the limiting parabola shown in Fig. 3, $kurt = \frac{3}{2}\, skew^2$. Therefore, let us now discuss the vertical offset *B*.

Let us study what the weak-multiplicative-noise approximation yields for *B*. That is, we again neglect the multiplicative noise contribution to the drift, resulting in a cancellation of $-\lambda_{eff} \approx -\lambda$. As discussed before, this weak noise approximation provides us with a lower limit of *B*, because $\left(-\lambda_{eff} + \frac{1}{2}(\phi\sigma_{F'})^2\right) / \left(-\lambda_{eff} + \frac{3}{2}(\phi\sigma_{F'})^2\right) \geq 1$. Again, note that there exists an upper limit, $(\phi\sigma_{F'})^2 < \left(\frac{2}{3}\right)\lambda_{eff}$, for the strength of the multiplicative noise. Therefore, in general $B \geq 0$.

To summarize, having established the lower limits of *A* and *B,* we conclude that our SDE (6) results in $kurt \geq \frac{3}{2} skew^2$, in almost perfect agreement with observations. Therefore, we conclude that the SDE (6) captures the overall dynamics of global SST variability remarkably well. In particular, we come to the conclusion that the observed non-Gaussianity of SST anomalies is due to multiplicative noise rather than to nonlinearities in the deterministic part of the SST equation [as often assumed, e.g., Burgers and Stephenson (1999)].

5. Summary and conclusions

In this paper we used a multiplicative noise model, directly derived from basic mixed-layer dynamics, to explain a very strong, observed constraint on the non-Gaussianity of global SST variability. The constraint is that the kurtosis is everywhere equal or larger than one-and-a-half times the squared skewness: $kurt \geq \frac{3}{2} skew^2$. As there is, to our knowledge, no obvious dynamical reason why SST variability should behave this way, the observational result itself is astonishing. We note that we are not the first investigators to observe such a constraint. Burgers and Stephenson (1999) observed for ENSO region SST anomalies that “kurtosis is positively correlated with the square of skewness” without discussing the dynamical implications. We think, however, that this is the first time that the relation of kurtosis versus skewness of SST anomalies has been shown globally and, more important, that a detailed dynamical explanation has been provided. The agreement between observations and our simple theory tells us that a univariate linear model with multiplicative noise captures the observed non-Gaussianity of SST anomalies almost all over the globe. This is consistent with a local study by Sura et al. (2006), which shows in detail that the non-Gaussianity at several OWS is captured by a multiplicative noise model. The bottom line is that a comprehensive (including multiplicative noise) stochastic approximation of the general mixed-layer SST equation is an excellent globally applicable model of anomalous SST variability.

Beside the dynamical clarification, why is it useful to know the observed relation between skewness and kurtosis of SST anomalies? First, it is useful as a benchmark for ocean models. Do ocean models simulate the correct non-Gaussian SST variability? An accurate representation of the non-Gaussian tails of SST distributions (extreme SST events) is crucial in the modeling and prediction of many important weather and climate phenomena, such as hurricanes, ENSO, NAO, etc. It is part of our current research to study if ocean models reproduce the observed relation between skewness and kurtosis for the correct physical reasons. To do so, we are planning to estimate the parameters of our stochastic mixed-layer model (6) from observations and model runs. A detailed comparison of observed and modeled parameters might reveal model deficiencies and could guide model development. Second, the equation $kurt \geq \frac{3}{2} skew^2$ is basically a forecasting tool for extreme SST anomalies. As we have discussed, kurtosis is a measure of how likely a non-Gaussian extreme event is. We have also seen that it is much easier to significantly estimate skewness from time series than kurtosis. That means, if we know the skewness of SST anomalies at a certain location, we can calculate the lower threshold of the expected kurtosis and, thereby, the likelihood of extreme anomalies for that location. Thus, our analysis of non-Gaussian SST statistics not only reveals some basic mechanisms of global SST variability, but should help constrain the likelihood of extreme SST anomalies in a forecasting environment.

Last but not least, we would like to stress the more general aspect of our analysis. Weather and climate risk assessment is about understanding the tails (extreme events) of probability density functions. We have shown that it is possible to develop stochastic models from first physical principles, which are capable of reproducing the observed statistics of extreme events. We, therefore, believe that sophisticated stochastic models (e.g., with multiplicative noise) are essential to model and understand extreme events in weather and climate, and hope that this paper may serve as an example how to combine observations with advanced theory to gain a better understanding of weather/climate related risk.

Acknowledgments. The authors thank two anonymous reviewers whose comments greatly improved the paper. This work was partly supported by NSF grant 0552047 "The impact of rapidly-varying heat fluxes on air-sea interaction and climate variability" and partly by NOAA's Climate Program Office.

References

Blaauboer, D., G. J. Komen, and J. Reiff, 1982: The behaviour of the sea surface temperature (SST) as a response to stochastic latent- and sensible heat forcing. *Tellus*, **34**, 17–28.

Burgers, G., and D. B. Stephenson, 1999: The "normality" of El Niño. *Geophys. Res. Lett.* **28**, 1027-1030.

Dinsmore, R. P., 1996: Alpha, Bravo, Charlie… Ocean weather ships 1940-1980. *Oceanus*, **39**, 9-10.

Frankignoul, C., 1985: Sea surface temperature anomalies, planetary waves, and air-sea feedback in the middle latitudes. *Rev. Geophys.* **23**, 357–390.

Frankignoul, C., and K. Hasselmann, 1977: Stochastic climate models. Part II. Application to sea-surface temperature anomalies and thermocline variability. *Tellus* , **29**, 289–305.

Gardiner, C. W., 2004: *Handbook of Stochastic Methods for Physics, Chemistry and the Natural Science, Third Edition*. Springer-Verlag, 415 pp.

Hall, A., and S. Manabe, 1997: Can local linear stochastic theory explain sea surface temperature and salinity variability? *Climate Dyn.*, *13*, 167–180.

Hasselmann, K., 1976: Stochastic climate models. Part I. Theory. *Tellus*, **28**, 473–484.

Horsthemke, W., and R. Léfèver, 1984: *Noise Induced Transitions: Theory and Applications in Physics, Chemistry, and Biology*. Springer-Verlag, 318 pp.

Kloeden, P., and E. Platen, 1992: *Numerical Solution of Stochastic Differential Equations*. Springer-Verlag, 632 pp.

Müller, D., 1987: Bispectra of sea-surface temperature anomalies. *J. Phys. Oceanogr.*, **17**, 26-36.

Paul, W., and J. Baschnagel, 1999: *Stochastic Processes: From Physics to Finance.* Springer-Verlag, 231 pp.

Peinke, J., F. Böttcher, and S. Barth, 2004: Anomalous statistics in turbulence, financial markets and other complex systems. *Ann. Phys.*, **13**, 450–460.

Reynolds, R. W., 1978: Sea surface temperature anomalies in the North Pacific Ocean. *Tellus*, **30**, 97–103.

Reynolds, R. W., T. M. Smith, C. Liu, D. B. Chelton, K. S. Casey, and M. G. Schlax, 2007: Daily high-resolution blended analyses for sea surface temperature. *J. Climate*, in press.

Sura, P., and M. Newman, 2007: The impact of rapid wind variability upon air-sea thermal coupling. *J. Climate*, in press.

Sura, P., M. Newman, and M. A. Alexander, 2006: Daily to decadal sea surface temperature variability driven by state-dependent stochastic heat fluxes. *J. Phys. Oceanogr.*, **36**, 1940-1958.

Sura, P., M. Newman, C. Penland, and P. D. Sardeshmukh, 2005: Multiplicative noise and non-Gaussianity: A paradigm for atmospheric regimes? *J. Atmos. Sci.*, **62**, 1391–1409.

Wilkins, J. E., 1944: A note on skewness and kurtosis. *Ann. Math. Stat.,* **15**, 333–335.

Figure Captions

Fig. 1: Skewness of SST anomalies for extended summer (upper panel) and winter (lower panel).

Fig. 2: Kurtosis of SST anomalies for extended summer (upper panel) and winter (lower panel).

Fig. 3: Scatter plot of kurtosis versus skewness for all data points equatorward of 65° North and South. Here we have not made any distinction between extended summer and winter, but plotted all available points. The solid line denotes the function $kurt = \frac{3}{2} skew^2$. The estimated local 95% confidence intervals on the values are indicated in the upper right corner of the figure.

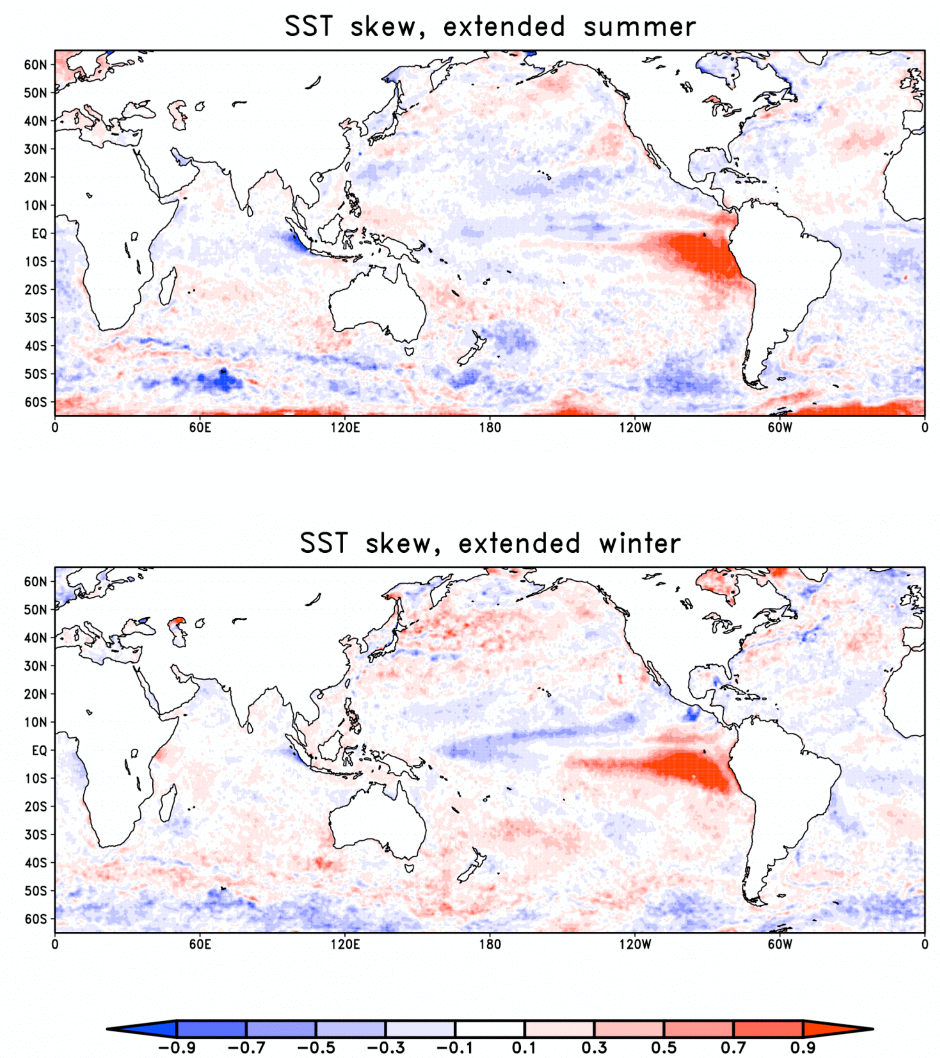

Fig. 1: Skewness of SST anomalies for extended summer (upper panel) and winter (lower panel).

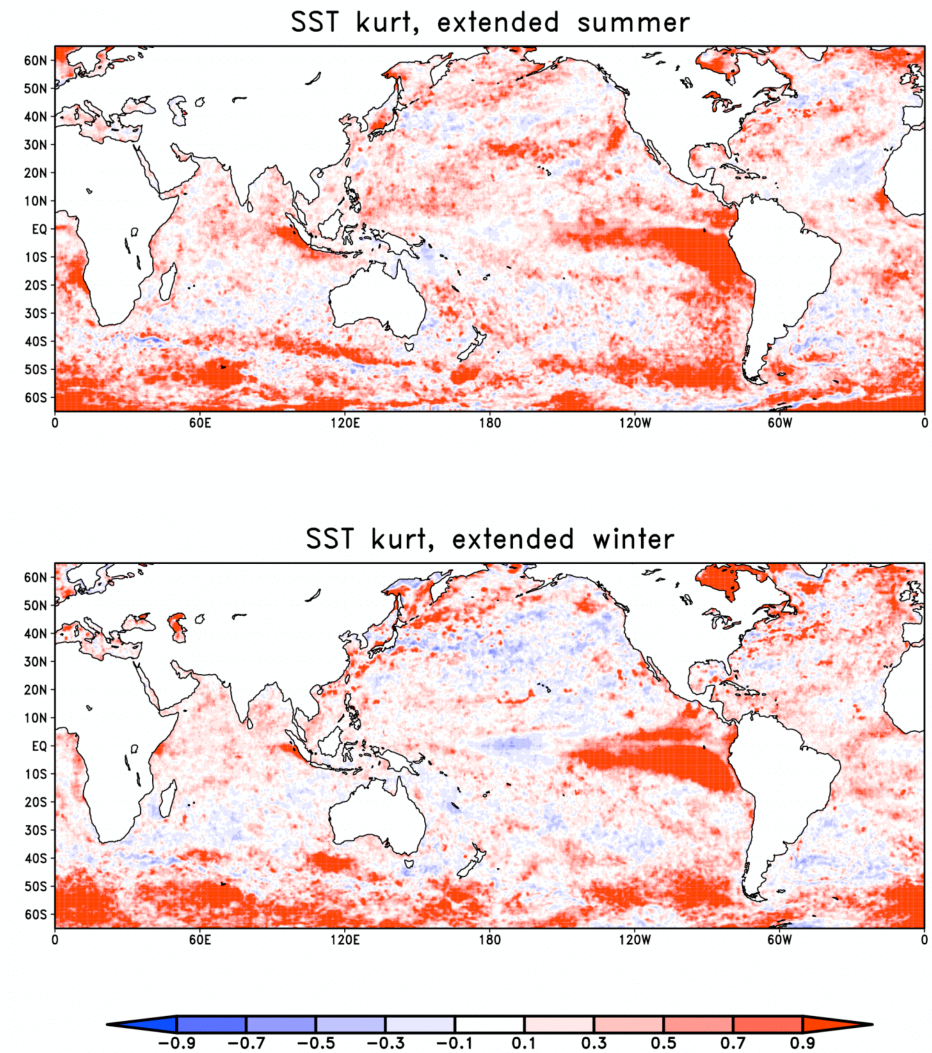

Fig. 2: Kurtosis of SST anomalies for extended summer (upper panel) and winter (lower panel).

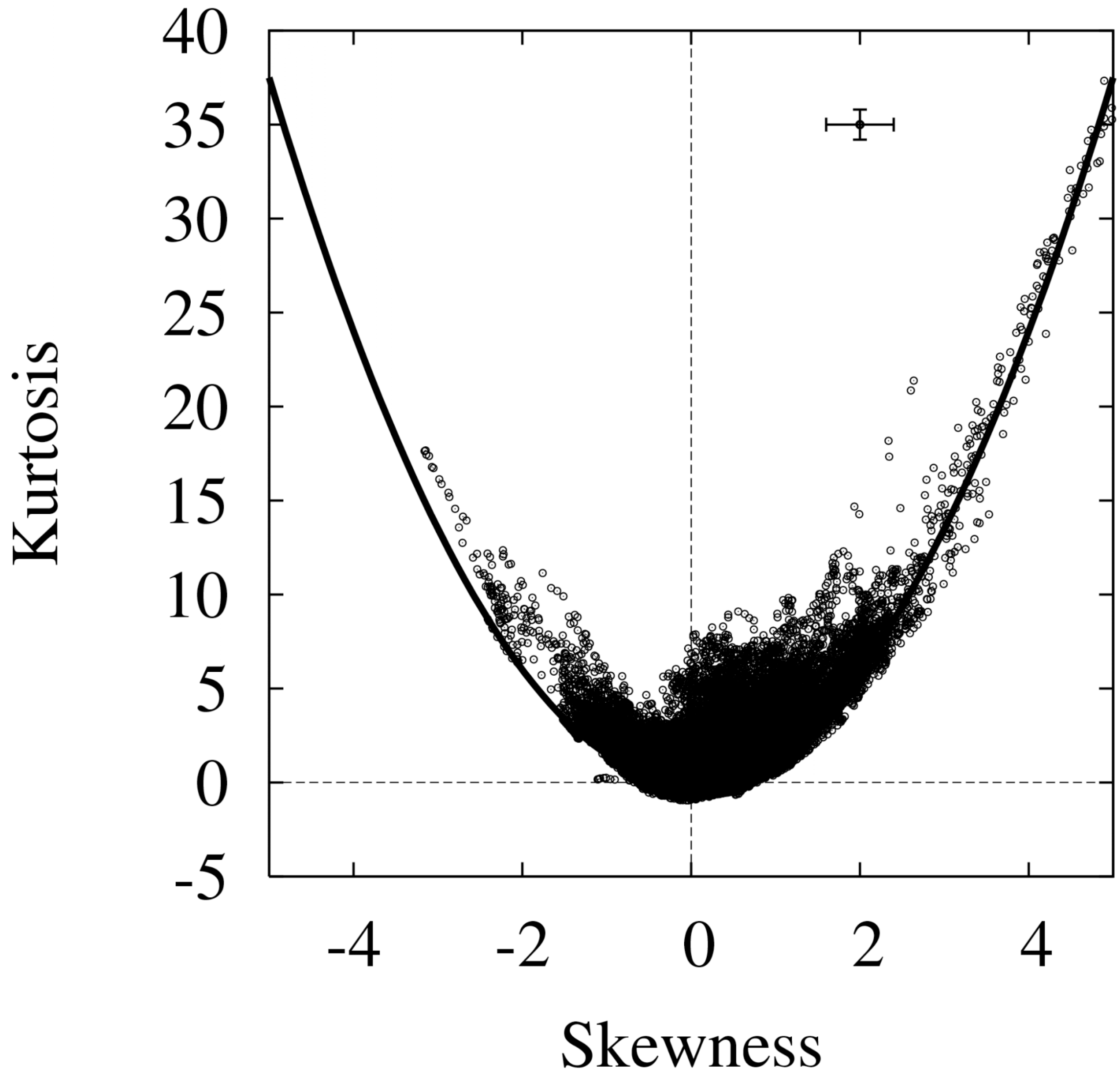

Fig. 3: Scatter plot of kurtosis versus skewness for all data points equatorward of 65° North and South. Here we have not made any distinction between extended summer and winter, but plotted all available points. The solid line denotes the function $kurt = \frac{3}{2} skew^2$. The estimated local 95% confidence intervals on the values are indicated in the upper right corner of the figure.